J. Fluid Mech. (2002), *vol.* 461, *pp.* 277–300.
DOI: 10.1017/S0022112002008388 Printed in the United Kingdom

Drag and lift forces on a bubble rising near a vertical wall in a viscous liquid

By FUMIO TAKEMURA[1], SHU TAKAGI[2], JACQUES MAGNAUDET[3] AND YOICHIRO MATSUMOTO[2]

[1]Graduate School of Frontier Sciences, The University of Tokyo, 7-3-1 Hongo, Bunkyo, Tokyo 113-0033, Japan

[2]Department of Mechanical Engineering, The University of Tokyo, 7-3-1 Hongo, Bunkyo, Tokyo 113-8656, Japan

[3]Institut de Mecanique des Fluides de Toulouse, UMR CNRS/INPT/UPS 5502, 2, Avenue Camille Soula, 31400 Toulouse, France

(Received 15 July 2001 and in revised form 3 January 2002)

The two components of the force acting on a clean almost spherical bubble rising near a plane vertical wall in a quiescent liquid are determined experimentally. This is achieved by using an apparatus in which a CCD camera and a microscope follow the rising bubble. This apparatus allows us to measure accurately the bubble radius, rise speed and distance between the bubble and the wall. Thereby the drag and lift components of the hydrodynamic force are determined for Reynolds numbers Re (based on bubble diameter, rise velocity U, and kinematic viscosity ν) less than 40. The results show the existence of two different regimes, according to the value of the dimensionless separation L^* defined as the ratio between the distance from the bubble centre to the wall and the viscous length scale ν/U. When L^* is $O(1)$ or more, experimental results corresponding to Reynolds numbers up to unity are found to be in good agreement with an analytical solution obtained in the Oseen approximation by adapting the calculation of Vasseur & Cox (1977) to the case of an inviscid bubble. When L^* is $o(1)$, higher-order effects not taken into account in previous analytical investigations become important and measurements show that the deformation of the bubble is significant when the viscosity of the surrounding liquid is large enough. In this regime, experimental results for the drag force and shape of the bubble are found to agree well with recent theoretical predictions obtained by Magnaudet, Takagi & Legendre (2002) but the measured lift force tends to exceed the prediction as the separation decreases.

1. Introduction

Understanding interactions between bubbles and solid walls is of importance for predicting how bubbly flow characteristics, such as void fraction and statistical distribution of bubble sizes, are affected by the presence of solid boundaries. When the bubble volume fraction becomes of $O(10^{-2})$, bubbles start to affect significantly the flow by providing a significant source of momentum and modifying the density of the bubbly mixture in an inhomogeneous fashion. Then the near-wall velocity distribution and the stability of the boundary layer become affected by the presence of the dispersed phase. Therefore, determining the forces acting on bubbles rising

near a wall is important for designing and predicting the efficiency of many processes involving bubbly flows. In the present work we focus on this question by considering the canonical case of a single bubble rising near a vertical wall in a quiescent liquid. We limit our investigation to the range of low-to-moderate particle Reynolds numbers where bubbles rising in common liquids are almost spherical.

Provided the distance L between the particle centre and the wall is much larger than the particle radius R, the drag force acting on a spherical particle moving parallel to a fixed infinite plane wall can be obtained analytically under Stokes approximation using the technique of reflections (Happel & Brenner 1973, pp. 58–95). In the opposite limit $L \approx R$, the lubrication approximation can be employed to evaluate the leading-order contribution to the drag (Goldman, Cox & Brenner 1967). The connection between these two approaches has been carefully studied using matched asymptotic expansions by Goldman *et al.* (1967) and O'Neill & Stewartson (1967). Nevertheless, the Stokes approximation does not provide a complete picture of wall–particle interactions since a spherical particle cannot experience any lift force in the Stokes regime (Bretherton 1962). Therefore, evaluating the migration or lift force acting on a non-deformable particle rising or falling parallel to a plane wall or to the streamlines of a pure shear flow in the low-Reynolds-number regime requires small inertia effects to be taken into account. Based on this idea and on the use of matched asymptotic expansions, Saffman (1965) obtained the lift force acting on a spherical particle migrating in a simple unbounded shear flow in the limit where advective effects due to the shear are much stronger than those due to the relative velocity between the particle and the fluid. Saffman's expression for the lift force was later extended by McLaughlin (1991) to the case where advection by the relative velocity is not negligible, and it was generalized to drops of arbitrary viscosity by Legendre & Magnaudet (1997) (see Stone 2000 for a review of further developments of Saffman's 1965 theory).

A large amount of work has been devoted to the analytical determination of hydrodynamic forces acting on a solid spherical particle moving parallel to a plane wall in the low-but-finite Reynolds number regime. Most of the studies made use of the technique of matched asymptotic expansions and estimated the two components of the force at first order in terms of the particle Reynolds number. Vasseur & Cox (1976) and Cox & Hsu (1977) considered the case where the wall lies in the inner (Stokes) region of the particle-induced flow, whereas Vasseur & Cox (1997) treated the situation where the wall lies in the outer (Oseen) region. The case of Couette and Poiseuille flows in which the inertial migration results from the interaction of the two walls with a uniform or non-uniform shear was first considered by Ho & Leal (1974). Since then, it has been the subject of several investigations, as well as the case where the particle moves in a simple shear flow in the presence of a single wall. The corresponding contributions differ by the various assumptions on which they are based, especially whether the particle is regarded as neutrally or non-neutrally buoyant and whether the wall lies in the Stokes or the Oseen region of the flow disturbance. A comprehensive review of these contributions and of their range of validity is given by Hogg (1994).

While there can be no lift force on a spherical bubble or drop moving in the Stokes flow regime, such a force may appear in the absence of inertia if the drop deforms due to the local viscous stress. In this case, the crucial parameter to be considered is the capillary number Ca expressing the ratio of the characteristic viscous stress to the capillary pressure. If the bubble rises near a wall, the flow field around it results from the superposition of the field corresponding to an unbounded fluid and that produced by the mirror image of the bubble with respect to the wall. The latter

contribution includes a finite strain which induces the deformation of the bubble for finite values of Ca, resulting in a non-zero transverse force. Numerous analytical studies concerning the deformation of a fluid sphere in a shear flow have been carried out under the Stokes approximation; early results are reviewed by Leal (1980). One of the most noticeable contributions including wall effects is that of Chan & Leal (1979) who determined the deformation of a neutrally buoyant drop of arbitrary viscosity moving in a Couette flow or in a plane Poiseuille flow of a non-Newtonian fluid. They compared their analytical predictions for the transverse migration speed and the equilibrium position of the drop in the flow with experimental results obtained by Karnis & Mason (1967); later they performed new experiments (Chan & Leal 1981) that confirmed, at least qualitatively, their predictions. Shapira & Haber (1988, 1990) determined the drag force and the deformation of a drop moving in a quiescent liquid and in a plane Couette flow, respectively. Uijttewaal, Nijhof & Heethaar (1993) and Uijttewaal & Nijhof (1995) used a boundary integral technique to obtain the deformation and the migration speed of a drop moving in a simple shear flow near a wall. Some of their results showed good agreement with available predictions whereas others, especially those related to transverse migration, revealed significant differences with available theories as well as with experiments performed by Smart & Leighton (1991) in a rotating Couette flow.

Few detailed experiments devoted to the near-wall motion of solid or fluid particles in a quiescent fluid have been reported. According to the review in Clift, Grace & Weber (1978), most of the early investigations considered the case of solid or fluid particles moving along the axis of a vertical cylinder; there the wall-induced correction to the particle velocity was expressed as a function of the ratio of the particle diameter to the tube diameter. A detailed study of the influence of a wall on the drag of a small solid sphere was performed by Ambari, Gauthier-Manuel & Guyon (1983). They maintained a falling sphere at a constant distance from a vertical wall by using a magnetic levitation technique and determined the evolution of the drag force *vs.* the distance to the wall in the low-Reynolds-number regime. Their results showed a good agreement with Faxén's expression (see Happel & Brenner 1973, pp. 326–327) for dimensionless gaps ranging from 10^{-2} to $O(1)$. A pioneering experiment was performed by Vasseur & Cox (1977) in order to determine the lateral migration of small solid particles falling between two parallel walls. Using optical techniques, they found good agreement with their theory in the case where the wall is located in the Oseen region of the flow disturbance.

This brief review suggests that most of the available experimental information about wall-induced effects concern either solid particles or drops moving in Couette and Poiseuille flows. In particular it seems that no precise determination of the lateral migration of drops and bubbles moving in a quiescent liquid has been carried out. Moreover, no systematic investigation of wall-induced effects has been reported in the range of intermediate Reynolds numbers where inertial effects are dominant while bubbles still maintain an almost spherical shape. The purpose of the present contribution is to fill part of this gap by using appropriate optical techniques and comparing experimental results for the drag and lift components of the force with analytical predictions.

2. Experimental apparatus and procedure

Figure 1 shows a diagram of the experimental facility used to measure the evolution of the bubble radius R, rise velocity U, wall-normal velocity W, and distance

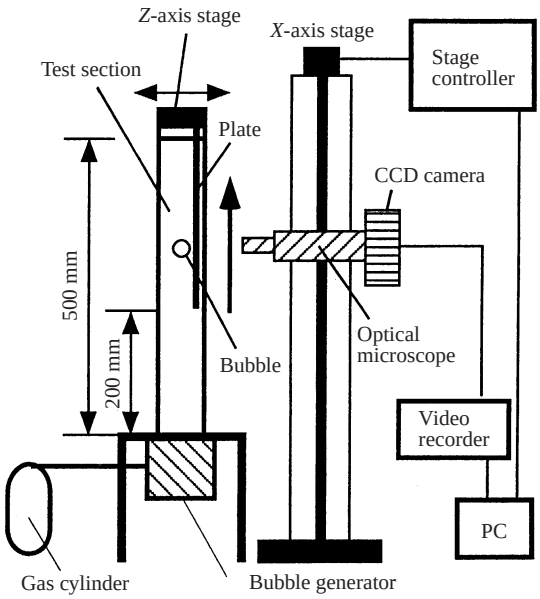

FIGURE 1. Sketch of the experimental device.

between the bubble centre and the wall L. Single bubbles are generated by a bubble generator connected to an air tank; the reader is referred to Takemura & Yabe (1999) for a precise description of this generator. The pressure inside the air tank is kept around 0.5 kPa higher than that within the liquid contained at the bottom of the test section. The test section is a 500 mm long glass channel with a square cross-section of $50 \times 50\,\mathrm{mm}^2$. The vertical wall is a stainless steel plate 300 mm long and 40 mm wide inserted in the middle of the cross-section (the possible influence of the outer wall of the device will be addressed during the discussion of the results). The vertical plate is connected to a horizontal (z) displacement system with a travelling distance of ± 20 mm; this system is used to adjust the distance between the bubble and the wall. The plate is suspended from the horizontal displacement system which rests on the top of the test section. The leading edge of the plate is located 200 mm above the bottom of the test section in order to avoid disturbances just after bubble generation. The heart of the measuring system consists of an optical device developed by Takemura & Yabe (1998, 1999). This device is fixed on the vertical x-displacement system; it combines a CCD camera with a microscope in order to measure accurately the radius of the bubble. Using this apparatus, Takemura & Yabe (1998) were able to obtain the drag force on a rising bubble with an accuracy better than 5%. The CCD camera has 640×480 pixels which, according to the calibration used in the present study, yields a resolution of about 6.4 μm per pixel. The depth of field of the microscope is about 150 μm.

To track the rising bubble, we adjust the speed of the camera as follows. A picture of the bubble is recorded on the personal computer via the video capture board at a rate of 30 frames per second. A binary image is made and the position of the bubble is determined. Then we calculate the relative speed of the bubble and the camera from consecutive frames and we use this relative speed to adjust the speed of the vertical displacement system. To determine the effect of the wall on the bubble motion, it is crucial to set the plate vertically. To ensure verticality, we proceed as follows. We first generate a bubble in the absence of the plate and let the camera follow it. Then we

	K2	K5	K10	K20	K50	K100
$\rho(\mathrm{kg\,m^{-3}})$	868	906	931	947	953	962
$\mu(\mathrm{kg\,m^{-1}\,s^{-1}} \times 10^3)$	1.99	4.44	9.32	18.9	44.7	94.0
$\nu(\mathrm{m^2\,s^{-1}} \times 10^6)$	2.3	4.9	10.0	20.0	46.9	99.5
$\sigma(\mathrm{kg\,s^{-2}} \times 10^3)$	18.3	19.7	20.1	20.8	20.8	20.9

TABLE 1. Physical properties of the silicone oils used in the experiments.

adjust the angle of the vertical displacement system in such a way that the camera captures the bubble along all its path within $\pm 25\,\mu\mathrm{m}$ in the horizontal direction. Finally we insert the plate in the test section and adjust its angle so that it is always located at the same position in the image, whatever the vertical distance from the leading edge.

All the experiments are carried out at room temperature and atmospheric pressure using silicone oil (dimethyl siloxane polymer; Shinetsu Chemical Co., KF-96) as the carrying liquid. To cover a sufficiently wide range of Re ($Re = 2RU/\nu$, where ν is the kinematic viscosity), we employ six different qualities of silicone oil with kinematic viscosities ranging from about 2.0×10^{-6} to $1.0 \times 10^{-4}\,\mathrm{m^2\,s^{-1}}$. The physical properties of these oils are detailed in table 1; hereinafter these various oils are referred to as K2 to K100, according to the denomination specified in table 1. Variations of oil viscosity with temperature are determined using a rotating Couette viscometer and corresponding corrections are taken into account in the analysis of the data. The temperature of the device is determined before and after each set of experiments in order to ensure that no significant temperature variation has occurred. An important property of silicone oil is its non-polar nature. Because of this, no indication of surface contamination has been detected in our experiments. In particular, the values of the drag force acting on bubbles rising far from the wall always agree with values corresponding to clean bubbles with a surface subject to a shear-free boundary condition (see below).

Using the device and the adjustments described above, the bubble radius, rise speed and distance between the bubble and the wall are measured from the recorded pictures and the time history of the camera speed. The radius and the distance L to the wall are evaluated on each frame while the local speed of the bubble is obtained by locating the centre of the bubble on each frame, calculating the relative speed from the movement of the centre in two consecutive frames, and adding the speed of the camera corresponding to these two frames. We fit the time history of L with polynomial functions of time up to fourth order and calculate the time rate of change of this fitting function in order to estimate the migration speed W in the direction perpendicular to the wall. The correlation is better than 0.995 for each curve and the maximum deviation between the fitted and experimental values is less than 2%.

Determining L precisely in cases where the bubble is not perfectly spherical requires the position of the bubble centroid to be properly defined. For this purpose, we choose an initial approximation of the centroid location (defined as $r = 0$), express the bubble contour as $r = g(\theta)$, and perform a Fourier decomposition of this contour (see figure 13). In such a decomposition, terms in $\cos\theta$ and $\sin\theta$ are associated with a translational mode and become zero if the origin $r = 0$ coincides with the geometrical centroid. We apply this condition iteratively to reduce the strength of the translational mode and obtain the position of the centroid at convergence.

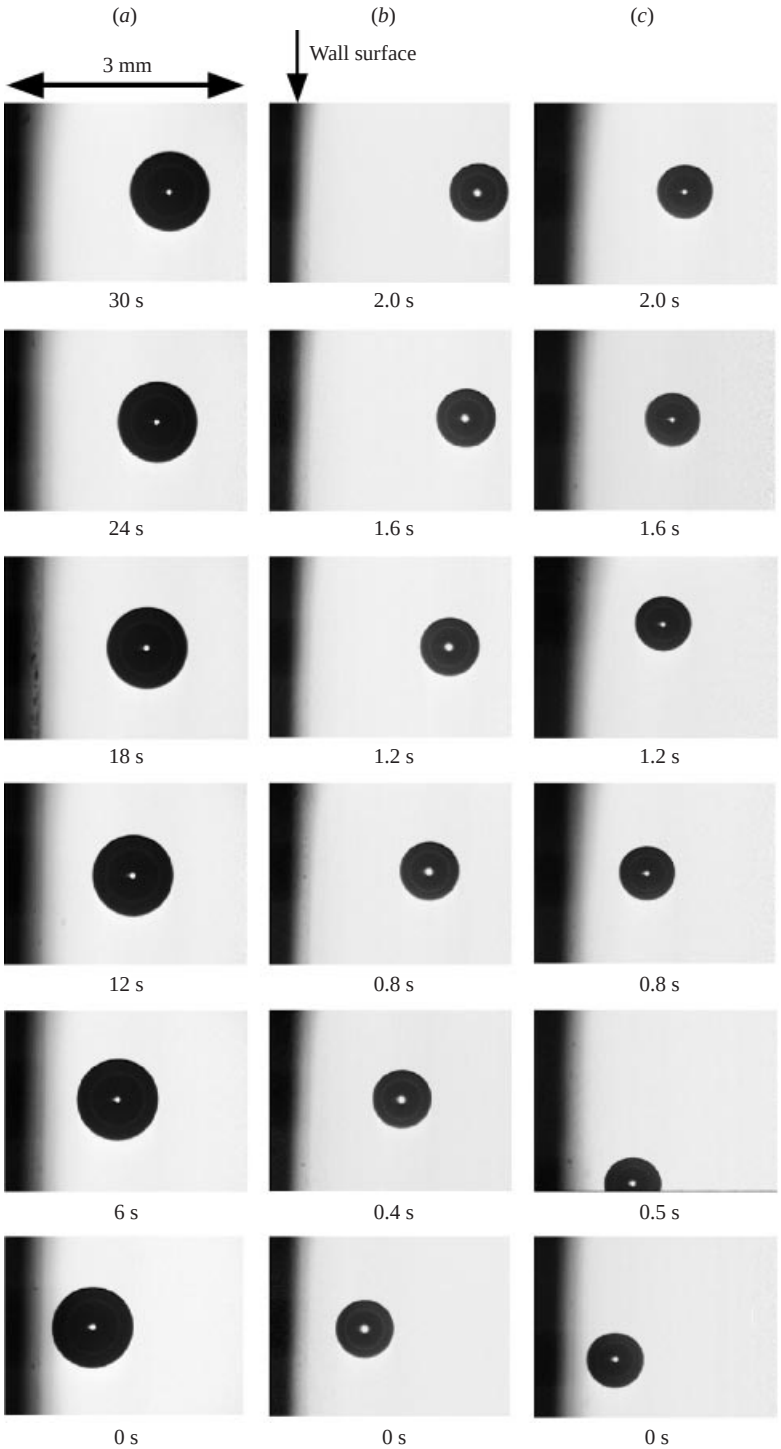

FIGURE 2. Photographs showing typical bubble trajectories near the wall. (*a*) K100: $R = 0.513\,\mathrm{mm}$, $U_\infty = 8.6\,\mathrm{mm\,s^{-1}}$, $Re = 0.09$; (*b*) K10: $R = 0.378\,\mathrm{mm}$, $U_\infty = 39.0\,\mathrm{mm\,s^{-1}}$, $Re = 3.0$; (*c*) K2: $R = 0.365\,\mathrm{mm}$, $U_\infty = 100.1\,\mathrm{mm\,s^{-1}}$, $Re = 32.0$.

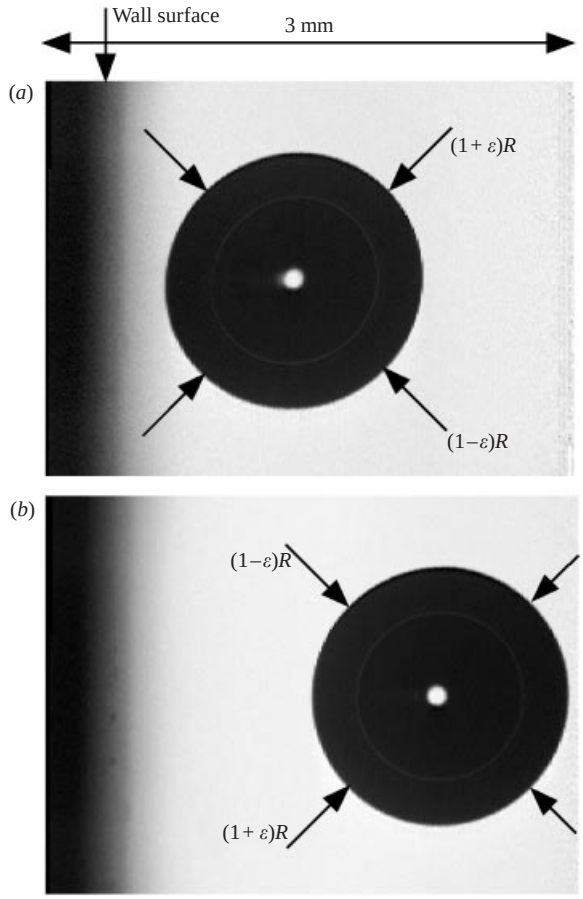

FIGURE 3. Two examples of slightly deformed bubbles rising near the wall. (*a*) $L/R = 1.50$, $\varepsilon = 0.017$; (*b*) $L/R = 2.57$, $\varepsilon = 0.0056$.

Figure 2 shows typical CCD camera photographs of bubbles rising near the plate taken in the K100, K10 and K2 silicone oils, respectively. The corresponding values of R, U_∞ (the rising speed far from the wall) and Re are given in the caption. Note that for K10 and K2 the total time from bottom to top is 2 s, whereas it is 30 s for the most viscous oil (K100). In all cases, the bubble migrates away from the wall and the migration speed decreases as the distance L to the wall increases. In K2 and K10 the bubble keeps an almost spherical shape and the deformation due to the wall is very small. In contrast, detailed observation of the bubble shape reveals that the deformation of bubbles rising in K100 may be significant. Figure 3 shows two typical photographs taken in this situation. The bubble radius is $R = 0.740$ mm, the rise velocity far from the wall is $U_\infty = 17.2\,\mathrm{mm\,s^{-1}}$ and the resulting value of the Reynolds number $Re_\infty = 2RU_\infty/\nu$ is 0.25. Case (*a*) corresponds to $L = 1.11$ mm and $U = 13.3\,\mathrm{mm\,s^{-1}}$, while case (*b*) corresponds to slightly larger values, namely $L = 1.90$ mm and $U = 15.0\,\mathrm{mm\,s^{-1}}$. It can be seen that both bubbles deform and there is no doubt that the shear induced around the bubble by the non-slip condition at the wall is responsible for this effect. In both cases one can observe that the bubble is lengthened (resp. shortened) along an axis inclined at $+45°$ (resp. $-45°$) from the horizontal. Assuming that the bubble deforms as an ellipsoid without volume change,

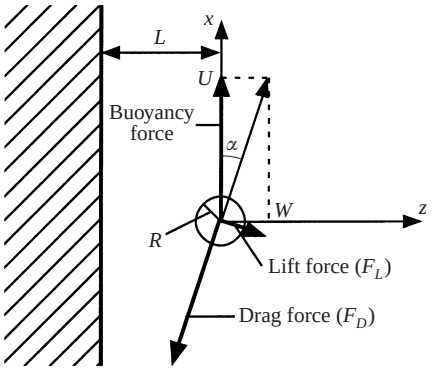

FIGURE 4. The force balance on the bubble.

we quantify its deformation ε by expressing the ratio ζ between the length of the major axis and that of the minor axis as $\zeta = (1+\varepsilon)/(1-\varepsilon)$. Using this definition we find $\varepsilon \approx 0.017$ in case (a) and $\varepsilon \approx 0.006$ in case (b). These values clearly indicate that the deformation increases as the bubble rises closer to the wall.

3. The wall-induced forces acting on a spherical bubble

3.1. *Estimates of the drag and lift forces*

The motion of a single bubble moving at finite Reynolds number is generally determined by writing a force balance involving various hydrodynamic effects assumed to act independently of each other. In an unbounded fluid these effects are usually separated into contributions corresponding to buoyancy, quasi-steady drag, history, pressure gradient, added mass and shear-induced lift, respectively (Magnaudet & Eames 2000). Since in the present experiment the fluid is at rest when the bubble is absent, forces due to pressure gradient and shear in the undisturbed flow are zero. In contrast, the added-mass force due to bubble acceleration and the history force may be significant when the bubble rises near the leading edge of the plate. To estimate the lowest location at which they can be neglected in the force balance, we performed some separate experiments in which we determined the time required by the bubble to reach a quasi-steady rise velocity when starting from rest in an unbounded fluid. In the range of Reynolds number corresponding to our experimental conditions, we found that this time is always less than $T_s = 0.1$ s. (T_s would be larger, especially at low Reynolds number, in the case of a rigid sphere because changing the shear-free boundary condition into a no-slip condition increases history effects (see Magnaudet & Eames 2000).) Near the leading edge of the plate, transient effects are less severe than in the former situation because the rise velocity changes only by 20% or less, compared to its value in unbounded fluid. Consequently we consider that the time period during which transient effects are important near the leading edge is at most T_s and we simply exclude from our data the first three frames corresponding to vertical distances from the leading edge less than $L_s = U_\infty T_s$.

Figure 4 shows a sketch of the force balance on the bubble as it rises steadily near the wall along a slightly inclined path; the drag, lift and buoyancy forces balance each other. Provided the inclination angle α is small, the wall-induced lift force almost balances the horizontal (z) component of the drag force. Therefore, if the drag law is known, this component of the drag can be determined from the experimental value of the transverse component W of the bubble velocity, yielding indirectly the

strength of the wall-induced lift force. Using the method of matched asymptotic expansions, Vasseur & Cox (1977) determined the drag and lift forces acting on a solid sphere migrating at low Reynolds number near a plane wall under conditions $R/L \ll Re \ll 1$. In the Appendix we show how their technique can be adapted to the case of a spherical inviscid bubble for which the no-slip condition at the surface is replaced by a shear-free condition. The resulting expression for the drag and lift components of the force depends on two dimensionless quantities, namely the Reynolds number Re and the dimensionless separation $L^* = LRe/(2R) = LU/v$ which can be interpreted as the ratio of the distance L between the bubble centre and the wall to the viscous length scale v/U. With this definition, it becomes clear that values of L^* larger (resp. smaller) than 1 correspond to situations where the wall lies in the Oseen (resp. Stokes) region of the disturbance produced by the bubble. From (A9) of the Appendix, we conclude that in the regime where Re and L^* are both small, the two components of the force balance on the bubble are

$$4\pi\mu RU\left(1+\frac{Re}{8}+\frac{3}{8}\frac{R}{L}\right)=\frac{4}{3}\pi R^3\rho g, \quad 4\pi\mu RW\left(1+\frac{3}{4}\frac{R}{L}\right)=\frac{Re}{8}\pi\mu RU, \qquad (1a,b)$$

where ρ and g denote the liquid density and gravity, respectively. (Strictly speaking, ρ is the density difference between the two fluids but the density of air is negligibly small in the present context.) Equations (1) simply state that the drag force in the vertical direction balances the net buoyancy force, whereas the drag force in the lateral direction balances the lift force produced by the combination of inertia effects and asymmetry of the wall-induced flow. Since the buoyancy force does not depend on the distance to the wall, the left-hand side of the first of (1a) is constant. Thereby we can write a relation between the local Reynolds number Re of the bubble rising at a distance L from the wall and the Reynolds number Re_∞ of the same bubble rising in an unbounded fluid:

$$Re\left(1+\frac{Re}{8}+\frac{3}{8}\frac{R}{L}\right)=Re_\infty\left(1+\frac{Re_\infty}{8}\right). \qquad (2)$$

For arbitrary values of L^*, the dimensionless wall-induced forces are given by complicated integrals. Consequently we generalize (1) and (2) to the form

$$F_{Dx}^{\infty}(Re)+2\pi\mu RU\,ReI_{Dx}(L^*)=F_{Dx}^{\infty}(Re_\infty), \qquad (3a)$$

$$F_{Dz}^{\infty}(Re)+2\pi\mu RW\,ReI_{Dz}(L^*)=2\pi\mu RU\,ReI_L(L^*), \qquad (3b)$$

where I_{Dx}, I_{Dz}, and I_L are the normalized wall-induced forces given by (A5)–(A7), and $F_{Dx}^{\infty}(Re)$ and $F_{Dz}^{\infty}(Re)$ are the algebraic values of the x- and z-components of the drag that the bubble would experience in an unbounded fluid if rising with the same angle α and the same Reynolds number Re. Figures 5 and 6 display the evolution of L^*I_{Dx}, L^*I_{Dz} and I_L as a function of L^*. Both figures show that all three quantities decrease as L^* increases and have a maximum gradient around $L^*=1$. They also suggest that wall effects become insignificant for $L^*>10$.

Equations (1) and (3) show that in the low-Re limit, forces acting on the bubble can be expressed as the sum of the drag force in unbounded fluid plus wall-induced forces proportional to Re. When Re becomes $O(1)$, there is obviously no rigorous proof that such a sum gives the correct total force. Nevertheless it is still possible to define the wall-induced correction as the difference between the actual value of the force and its value at the same Reynolds number in an unbounded fluid. Therefore, to estimate $F_{Dx}^{\infty}(Re)$ and $F_{Dz}^{\infty}(Re)$ at a finite Reynolds number, we use the correlation

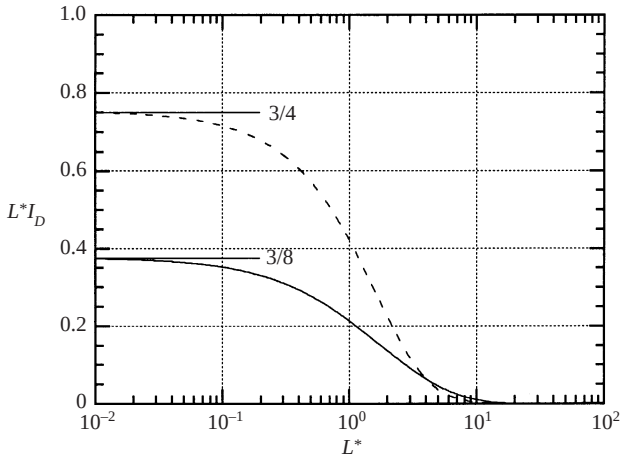

FIGURE 5. The wall-induced corrections to the drag force in the regime $Re_\infty \ll 1$, $L^* \gg 1$. Solid line: L^*I_{Dx} (equation (A 5)); dashed line: L^*I_{Dz} (equation (A 7)).

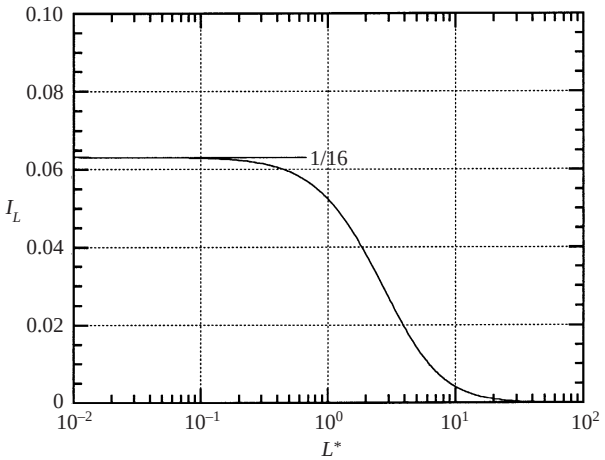

FIGURE 6. The wall-induced lift force I_L in the regime $Re_\infty \ll 1$, $L^* \gg 1$ (equation (A 6)).

proposed by Mei, Klausner & Lawrence (1994), namely

$$\frac{F_{Di}^{\infty}(Re)}{4\pi\mu R U_i} = f(Re) = 1 + \left\{ \frac{8}{Re} + \frac{1}{2}(1 + 3.315Re^{-1/2}) \right\}^{-1}, \tag{4}$$

where the index i stands for either of the directions x and z, and U_i stands for the corresponding velocity component (U or W). Note that strictly speaking the Reynolds number involved in (4) is $Re = 2R(U^2 + W^2)^{1/2}/\nu$; however U is always positive and W/U is always much smaller than unity in our experiments, so that the latter definition of Re almost coincides with our initial definition $Re = 2RU/\nu$. The correlation (4) agrees with the asymptotic solution found by Taylor & Acrivos (1964) in the low-Re regime and with the boundary-layer solution obtained by Moore (1963) in the high-Re regime. Experiments performed in organic liquids and numerical studies have shown that (4) is also a sound approximation of the drag at intermediate Reynolds numbers (Magnaudet & Eames 2000). We evaluated the velocity U_∞ of bubbles rising far from the plate by equating the drag force (4) with the buoyancy

force acting on the bubble. Comparing this estimate with the optical determination of U_∞ revealed a very good agreement. This allows us to conclude that bubbles remain clean in our experiments, i.e. no effect of contamination by surface-active impurities is discernible. Using (4), relation (2) may be generalized as

$$Re(f(Re) + \tfrac{1}{2}ReI_{Dx}(L^*, Re)) = Re_\infty f(Re_\infty). \tag{5}$$

Note that I_{Dx} is now *a priori* a function of both L^* and Re, since there is no reason to believe that the analytical expression established in the Appendix still holds for $O(1)$ Reynolds numbers. Once L, R, U and U_∞ have been measured, we determine Re_∞ and Re and use (5) to evaluate the wall-induced correction to the drag force in the form

$$L^* I_{Dx}(L^*, Re) = \frac{L}{R}\left(\frac{Re_\infty}{Re} f(Re_\infty) - f(Re)\right). \tag{6}$$

In the transverse direction, (3) and (4) imply

$$I_L(L^*, Re) = \frac{2\alpha}{Re}\left[f(Re) + \frac{R}{L} L^* I_{Dz}(L^*, Re)\right] = \alpha\left[\frac{2}{Re} f(Re) + I_{Dz}(L^*, Re)\right]. \tag{7}$$

Following a previous remark, we approximate the Reynolds number Re in (6) and (7) as $Re = 2RU/\nu$ because the angle α is always small. Moreover, to use (7) we need the further assumption that the correction I_{Dz} to the lateral drag force can be estimated using the analytical result (A7) whatever the Reynolds number. This assumption is reasonable because figure 5 shows that for a given L/R the wall-induced correction $L^* I_{Dz}(L^*, Re)$ becomes small when Re becomes larger than unity. Hence, even though the analytical estimate (A7) may not be accurate for such Reynolds numbers, the corresponding error should not have a significant influence on the value of the lift force. Moreover, results to be discussed in the next section suggest that predictions for the wall-induced drag derived in the limit of vanishingly small Reynolds number remain fairly accurate at least up to $Re = O(1)$.

The uncertainties affecting the various quantities determined in our experiments can be quantified as follows. The uncertainty on R is 1 pixel, i.e. about 6.4 μm, whereas that on L is about 30 μm because the wall is somewhat out of focus. The uncertainty in the relative speed of the bubble and the camera is about 0.4 mm s^{-1}, i.e. the error in the determination of U is about 4% when the bubble rises at 10 mm s^{-1}. In (5) the largest uncetainty comes from the angle α (i.e. from the transverse velocity W); the corresponding error is estimated to range from 10% to 25%. Using these estimates, we determined the uncertainties in quantities such as U/U_∞, L/R, I_{Dx} and I_L by using standard techniques (Benedict, Abernethy & Osolsobe 1985).

3.2. *The wall-induced drag force*

Figure 7(*a*) shows the values of $L^* I_{Dx}$ deduced from (4) for various values of Re_∞ ranging from 0.11 to 32.0. Experimental values corresponding to $Re_\infty = 0.62$ and 1.3 are in good agreement with the analytical solution derived in the Appendix. The agreement between the asymptotic solution and the experimental values corresponding to $Re_\infty = 1.3$ is noticeably good. It suggests that, although this Reynolds number is outside the strict range of validity of Oseen-type solutions, the $O(Re)$ terms taken into account in the asymptotic solution (A 5) still provide the dominant wall-induced contribution. In contrast, experimental values corresponding to $Re_\infty = 5.9$ and 32.0 clearly show that the low-Re solution underestimates the wall effect in this regime. In practice, the consequences of this underestimate are not very serious because figure 5

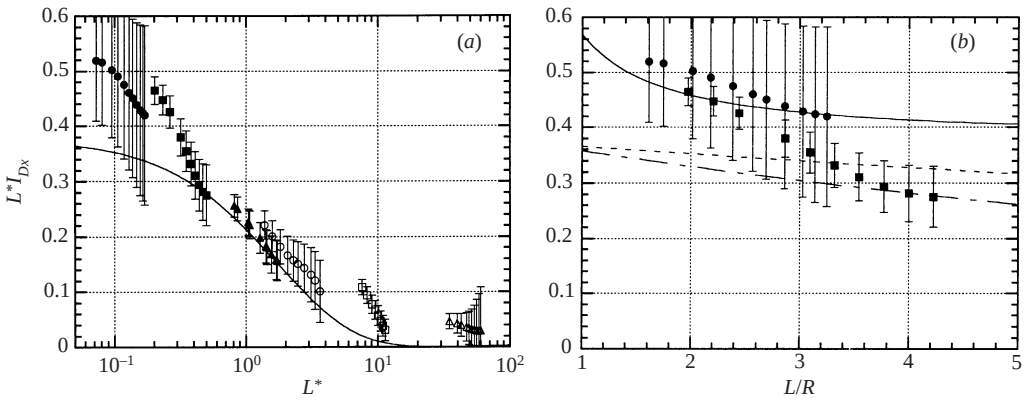

FIGURE 7. (*a*) The wall-induced drag correction $L^*I_{Dx}1$ *vs.* L^*. ●, $Re_\infty = 0.11$; ■, $Re_\infty = 0.25$; ▲, $Re_\infty = 0.62$; ○, $Re_\infty = 1.3$; □, $Re_\infty = 5.9$; △, $Re_\infty = 32.0$; ——, numerical integration of (A 5). (*b*) The wall-induced drag correction L^*I_{Dx} *vs.* L/R for $L^* < 1$. ●, $Re_\infty = 0.11$; ■, $Re_\infty = 0.25$; ——, equation (8); - - - -, numerical integration of (A 5) for $Re_\infty = 0.11$; — - —, numerical integration of (A 5) for $Re_\infty = 0.25$.

indicates that the relative contribution of the correction L^*I_{Dx} to (3) is weak when $L^* > 8$.

Results corresponding to the lowest two values of Re_∞ (0.11 and 0.25) reveal that wall effects become larger than predicted by the foregoing analytical solution when the bubble rises very close to the wall. This was to be expected since the condition $L^* \gg 1$ under which the solution (A 5) was derived is clearly not satisfied in this regime. Another asymptotic solution valid in the opposite limit $L^* \ll 1$ was recently obtained by Magnaudet, Takagi & Legendre (2002). The corresponding result for the drag correction is, in the present notation,

$$L^*I_{Dx} = \frac{3}{8} + \frac{9}{64}\frac{R}{L} + \frac{27}{512}\left(\frac{R}{L}\right)^2. \tag{8}$$

Figure 7(*b*) shows how the two series of data corresponding to $Re_\infty = 0.11$ and 0.25 compare with (8). Given the experimental uncertainty, the series for $Re_\infty = 0.11$ is found to agree closely with the analytical prediction over the whole range of L/R. This agreement shows that at such distances from the wall, the contribution of higher-order corrections to R/L taken into account in (8) is significant. By comparison with (A 8), this shows that the flow field is not satisfactorily represented by considering the bubble simply as a point force, as in the theories of Vasseur & Cox (1976, 1977) or in the solution derived in the Appendix. The behaviour of the series corresponding to $Re_\infty = 0.25$ is particularly interesting. Data obtained for the smallest values of L^* or L/R agree well with (8), while those corresponding to the largest separations agree with (A 5). The transition between the two asymptotic evolutions is smooth and takes place in the range $L^* \approx 0.3$–0.4.

At this point a crude evaluation of the possible influence of the outer wall of the device on the results is in order. The drag force acting on a bubble rising in a quiescent liquid between two parallel walls separated by a gap H was obtained by Shapira & Haber (1988). Their results, valid under the assumptions $L^* \ll 1$ and $H^* = HU/\nu \ll 1$, indicate that the relative contribution of the most distant wall to the wall-induced drag force is about 2.5% for $L/H = 0.125$. In our experiments H is 25 mm and the distance L is always less than 3 mm, implying that L/H is smaller

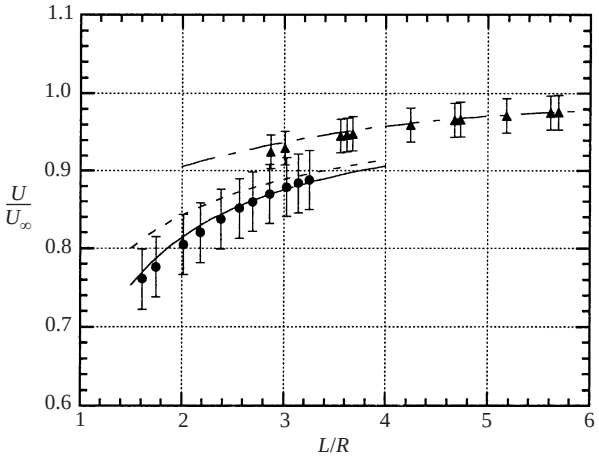

FIGURE 8. The relative rise velocity U/U_∞ *vs.* L/R. ●, $Re_\infty = 0.11$; ▲, $Re_\infty = 0.62$. Curves: numerical integration of (3) with $L^* I_{Dx}$ given by: ——, (8) for $Re_\infty = 0.11$; - - - -, (A 5) for $Re_\infty = 0.11$; — - —, (A 5) for $Re_\infty = 0.62$.

than 0.12. Then, using (8) and keeping in mind that data obtained in the regime $L^* \ll 1$ correspond to values of L/R less than 4, we conclude that the influence of the outer wall is very weak, being everywhere smaller than the first two terms on the right-hand side of (8).

Wall effects in the streamwise direction can also be evaluated by plotting the experimental values of the ratio U/U_∞ as a function of L/R. Given Re_∞, an analytical estimate of this ratio may also be obtained by solving (3) for Re, assuming that the wall-induced correction can be obtained from (A 5) whatever Re_∞. Figure 8 shows how this velocity ratio behaves for $Re_\infty = 0.11$ and 0.62. In the former case the rise velocity decreases severely as the distance to the wall decreases and the local rise velocity U is only 78% of U_∞ for $L/R \approx 1.8$. In line with the discussion of figure 7(b), this decrease of U is predicted well by (8), while it is underestimated by (A 5). Similarly, as could be expected from figure 7(a, b), the rise velocity of bubbles corresponding to $Re_\infty = 0.62$ is accurately predicted by (A 5) for large enough separations ($L/R > 3.5$, say) and is slightly overestimated by this expression for smaller separations.

Figure 9 shows the profiles of U/U_∞ corresponding to $Re_\infty = 5.9$ and 32.0. The difference between U and U_∞ is less than 3% everywhere. This trend confirms that, given L/R, the influence of the wall on the streamwise velocity becomes negligible when the Reynolds number is $O(10)$ or more. Hence, even though the analytical estimate of I_{Dx} is clearly in error for such Reynolds numbers (see the solid line in figure 9), this has little effect on the prediction of U. To summarize, figures 8 and 9 indicate that (3) combined with the analytical estimate (A 5) allows us to obtain a reasonable estimate of the reduction in the streamwise velocity of a bubble near the wall for $L^* > 0.35$. For smaller L^*, good predictions are obtained by using (8) in place of (A 5).

3.3. *The wall-induced lift force on a spherical bubble*

Figure 10 shows the reduced lift force I_L as a function of L^* for $Re_\infty = 0.6$, 0.8, 2.1 and 4.4. It appears that I_L is a monotonically decreasing function of L^* in this range of Re_∞, i.e. a decreasing function of L/R for a given Re_∞. Similarly, if the results corresponding to a given L/R were plotted as a function of Re, it would become

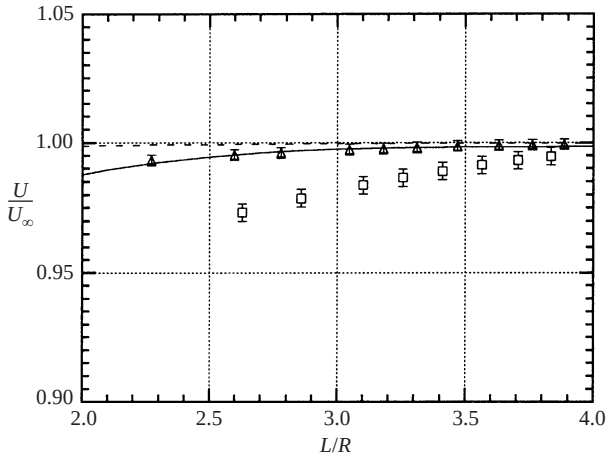

FIGURE 9. The relative rise velocity U/U_∞ *vs.* L/R. □, $Re_\infty = 5.9$; △, $Re_\infty = 32.0$. Numerical integration of (3) with $L^* I_{Dx}$ given by (A 5): ——, $Re_\infty = 5.9$; - - - -, $Re_\infty = 32.0$.

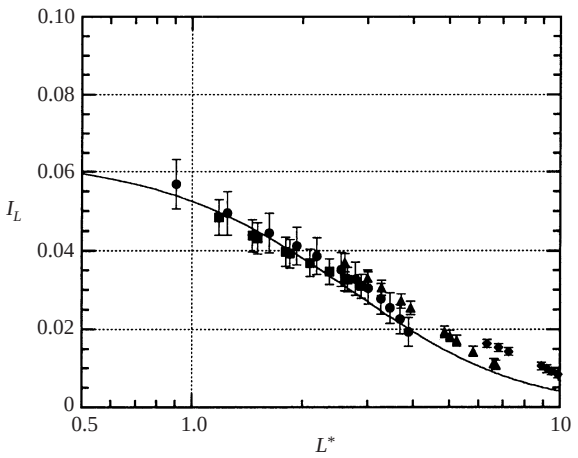

FIGURE 10. The wall-induced lift force I_L *vs.* L^* for $L^* > 1$. ●, $Re_\infty = 0.6$; ■, $Re_\infty = 0.8$; ▲, $Re_\infty = 2.1$; ◆, $Re_\infty = 4.4$; ——, numerical integration of (A 6).

apparent that I_L is a monotonically decreasing function of the Reynolds number. Results shown in figure 10 indicate that, up to $L^* \approx 3$, experimental values agree well with the analytical solution (A 6), even when the bubble Reynolds number is $O(1)$ (for $L^* = 2$ and $Re_\infty = 0.8$, the difference between the analytical prediction and the experimental value is about 12%). Again this suggests that, even though the asymptotic solution derived in the Appendix has been formally obtained under the assumption $Re \ll 1$, it is valid up to $Re = O(1)$ and $L^* = O(1)$. For larger values of L^* and Re_∞, figure 10 shows that the analytical solution underpredicts the lift force, as we have already observed for the drag correction in figure 7(*a*). This trend is confirmed by figure 11 in which we have plotted I_L for values of Re_∞ ranging from 5.5 to 32.0. For these values of Re_∞, L^* ranges from 10 to 60 approximately. The figure shows that experimental values are typically twice as large as analytical predictions in this range of Re_∞ and L^*. Combining the results of figures 10 and 11, we conclude that for $Re_\infty = O(1)$ or more, (A 6) underpredicts the migration velocity

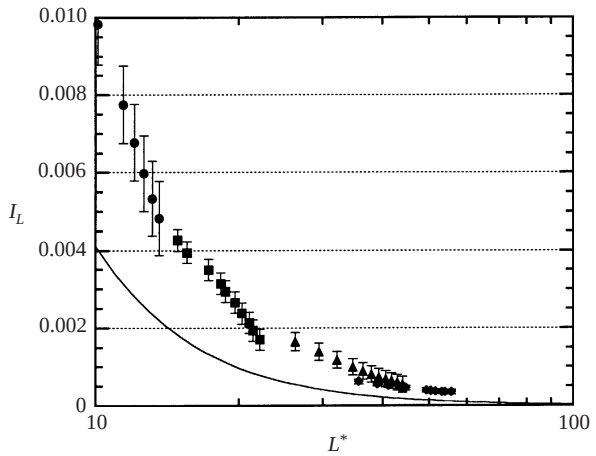

FIGURE 11. The wall-induced lift force I_L *vs.* L^* for $L^* > 1$. ●, $Re_\infty = 5.5$; ■, $Re_\infty = 7.3$; ▲, $Re_\infty = 15.0$; ◆, $Re_\infty = 32.0$; ——, numerical integration of (A 6).

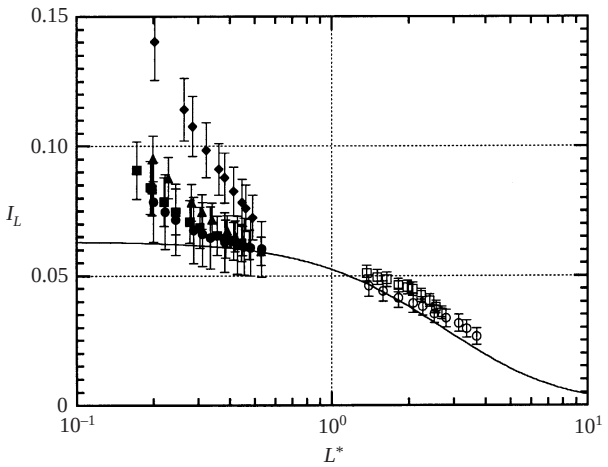

FIGURE 12. The wall-induced lift force I_L *vs.* L^* for $L^* < 1$ and $L^* > 1$. ■, $Re_\infty = 0.25$ in K10; ●, $Re_\infty = 0.25$ in K20; ▲, $Re_\infty = 0.25$ in K50; ◆, $Re_\infty = 0.25$ in K100; ○, $Re_\infty = 1.25$ in K20; □, $Re_\infty = 1.25$ in K50; ——, numerical integration of (A 6).

by a factor of two for $L^* \geqslant 4$. This underprediction certainly has minor consequences for large values of L^*, since the lift force vanishes whatever Re_∞ in the limit $L^* \to \infty$. In contrast, it may induce severe underpredictions of the migration velocity when L^* and Re_∞ are in the range 2–10. In this regime, full numerical solutions are required to obtain a uniformly valid expression of I_L.

4. The lift force on a slightly deformed bubble in the low-L^* regime

Figure 12 shows the reduced lift force I_L as a function of L^* for $Re_\infty = 0.25$ and 1.25. When the bubble is spherical, the lift force is a function of Re and L^* only, as we saw before. In contrast, if departures from sphericity are significant, the capillary number $Ca = \mu U/\sigma$ (μ being the dynamic viscosity and σ the surface tension) becomes a crucial parameter for the determination of the lateral migration (see Leal 1980). This is why for each of the above two Reynolds numbers we carried

out different sets of experiments by using oils with different viscosities. Figure 12 shows that, given Re_∞ and L^*, the values of I_L do not depend on the liquid viscosity when L^* is larger than unity and agree well with the asymptotic solution (A 6). This is a clear indication that, in the present range of viscosities, bubbles are almost spherical for $L^* > 1$. In contrast, two new features appear in the range $L^* < 1$.

First, the two series of experiments performed with the two least-viscous oils show a monotonic increase of I_L when L^* is decreased, whereas the analytical solution predicts an almost constant value for $L^* < 0.5$. Since the two series of values are almost identical in spite of the different viscosities, we conclude that the corresponding bubbles are almost spherical. Consequently these results suggest that the inertial migration increases more than predicted by (A 6) as the wall is approached. In the other two series performed in K50 and K100, the influence of the viscosity is manifested in a spectacular way and the lift force is much larger than predicted by (A 6). This suggests that the corresponding bubbles are deformed by the shear produced by the non-slip condition at the wall. Although this deformation remains small in our experiments (see figure 3), figure 12 indicates that it cannot be neglected in the prediction of the transverse force acting on the bubble in the low-L^* limit. This contrasts with the above discussion on the wall-induced drag correction, for which we found that the spherical approximation is suitable over the whole range of Re_∞ and L^*. The reason for this difference can be easily understood by examining the typical magnitude of the ratio I_L/I_{Dx} for a spherical bubble. According to (A 8), $I_L/I_{Dx} = L^*/6$ in the limit $Re \to 0$, $L^* \to 0$. Hence the transverse force induced by finite inertia effects is typically one to two orders of magnitude smaller than the correction experienced by the drag when $10^{-1} < L^* < 1$, which makes I_L much more sensitive to small deformations than I_{Dx}.

Motivated by the present experimental results, the deformation and lateral migration of bubbles and drops moving parallel to a wall in a quiescent liquid were recently analysed theoretically by Magnaudet *et al.* (2002) by combining the domain perturbation technique (Leal 1992, p. 223) with the method of reflections. This analysis was carried out for the case where the wall lies in the Stokes region of the flow disturbance, i.e. $L^* \ll 1$; it assumes $Ca \ll 1, Re \ll 1$, with $Re/Ca = O(1)$, so that effects of deformation and small inertia are taken into account in a consistent manner. At first order in Ca, the leading-order deformation makes the bubble ellipsoidal with a major axis directed along the first diagonal in the (x, z)-plane. Defining the length of the major/minor axis as $(1 \pm \beta)R$, Magnaudet *et al.* (2002) found that the deformation experienced by a bubble of negligible viscosity is

$$\beta = \frac{3}{8} Ca \left(\frac{R}{L}\right)^2 \left\{1 + \frac{3}{8}\frac{R}{L}\left(1 + \frac{3}{8}\frac{R}{L} + \frac{73}{64}\left(\frac{R}{L}\right)^2\right)\right\} + O\left(\left(\frac{R}{L}\right)^6\right). \qquad (9)$$

It is worth noting that this result is qualitatively identical to that obtained by Taylor (1934) in a simple unbounded shear flow. In other words, the bubble would adopt the same shape and orientation if it were maintained at rest in the simple shear flow $\boldsymbol{U} = (\beta/Ca)U(z/R)\boldsymbol{e}_x$.

We can obtain an estimate of the influence of the outer wall of the device on the deformation by comparing terms on the right-hand side of (9) with the effect of the second wall predicted by Shapira & Haber (1988). Their theory shows that the relative contribution of the most distant wall to the deformation is about 2.5% for $L/H = 0.125$. Then, using arguments similar to those developed in § 3.2, we conclude that the corresponding contribution is smaller than the first three terms within curly brackets in (9) for all locations at which we were able to measure the deformation.

No.	Oil	R (mm)	U (mm s^{-1})	L/R	Re	Ca	ε
1	K100	0.564	8.16	1.56	0.092	0.037	0.0080
2	K100	0.564	8.43	2.04	0.096	0.039	0.0045
3	K100	0.647	10.46	1.57	0.136	0.048	0.0120
4	K100	0.647	11.31	2.35	0.147	0.052	0.0038
5	K100	0.752	13.43	1.48	0.203	0.062	0.0172
6	K100	0.752	15.00	2.53	0.227	0.069	0.0056
7	K100	0.752	15.37	2.92	0.232	0.070	0.0035
8	K100	0.814	16.30	1.46	0.267	0.075	0.0226
9	K100	0.814	16.88	1.79	0.276	0.077	0.0138
10	K100	0.814	17.52	2.08	0.287	0.080	0.0103
11	K100	0.814	17.84	2.32	0.292	0.082	0.0079
12	K100	0.814	18.17	2.52	0.297	0.083	0.0063
13	K100	0.814	18.86	2.98	0.309	0.086	0.0036
14	K100	0.904	19.00	1.45	0.345	0.087	0.0233
15	K100	0.904	19.96	1.62	0.363	0.091	0.0198
16	K100	0.904	20.66	1.93	0.375	0.095	0.0132
17	K100	0.904	20.73	2.01	0.377	0.095	0.0120
18	K100	0.904	21.74	2.60	0.395	0.100	0.0077
19	K100	0.904	22.27	3.00	0.405	0.102	0.0043
20	K50	0.615	20.01	1.52	0.525	0.042	0.0108
21	K50	0.615	21.40	2.04	0.562	0.046	0.0049

TABLE 2. Experimental data used in figure 14.

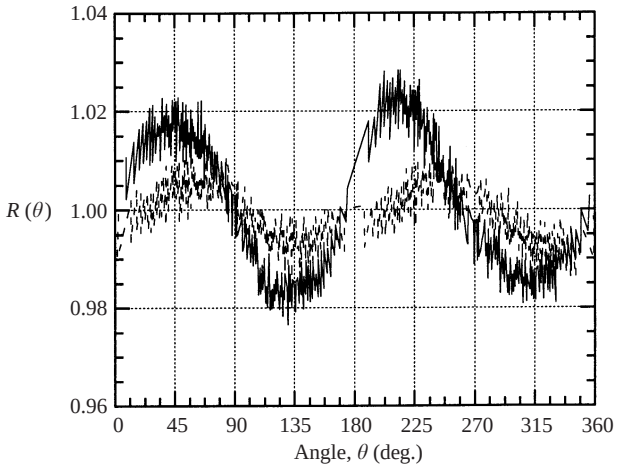

FIGURE 13. The local radius $R(\theta)$ of bubbles shown in figure 3 *vs.* the meridian angle θ. ——, figure 3(*a*); - - - -, figure 3(*b*).

Experimentally, we determined bubble deformation by using the pictures recorded for $0.092 < Re_\infty < 0.59$. The corresponding experimental data are reported in table 2. As indicated in § 2, a direct estimate of the deformation was obtained by determining the lengths L_M and L_m of the major and minor axes of the bubble. Setting $L_M = (1+\varepsilon)R$ and $L_m = (1-\varepsilon)R$ and assuming that ε is small, we approximated ε through the relation $2\varepsilon = L_M/L_m - 1$. We also performed a more complete determination by expanding the projection of the bubble contour in Fourier modes (figure 13). This second technique allowed us to identify higher-order deformation

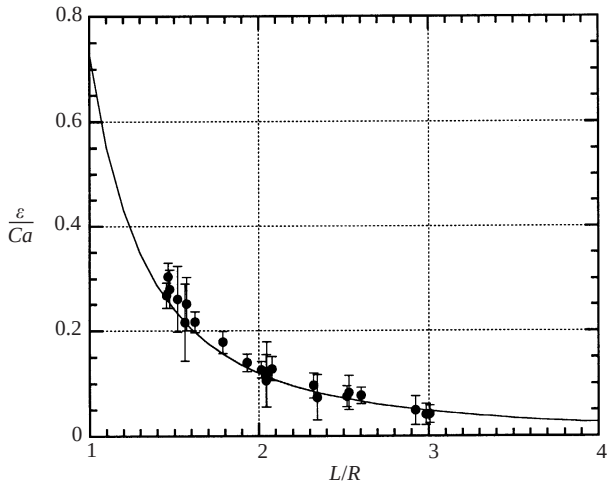

FIGURE 14. The normalised deformation ε/Ca *vs.* the relative separation L/R: ●, experimental values corresponding to data of table 2; ——, β/Ca from (9).

modes and to conclude that both determinations provide very similar amplitudes for the dominant mode. Figure 14 shows how ε/Ca evolves with the separation L/R and how it compares with the theoretical prediction β/Ca for the dominant mode. The deformation increases monotonically as the separation decreases, being about seven times larger for $L/R = 1.5$ than for $L/R = 3$. This confirms that the wall is entirely responsible for the observed shape. The measured deformation closely follows the prediction of (9) over the whole range of separations for which we were able to detect a significant departure from sphericity. However, there is a slight underprediction for the smallest separations reached in the experiments. This trend would probably become more pronounced in the limit $L/R \to 1$ because of the influence of higher-order terms neglected in (9).

Using the definition of the reduced lift force I_L given by (3) and introducing the Ohnesorge number $Oh = Re/Ca = 2\rho R\sigma/\mu^2$, the theoretical result obtained by Magnaudet *et al.* (2002) for the lateral migration may be expressed in the form

$$I_L = \frac{1}{16}\left\{1 + C_1\frac{R}{L} + C_2\left(\frac{R}{L}\right)^2 + C_3\left(\frac{R}{L}\right)^3 + \frac{12}{5}Oh^{-1}\left(\frac{R}{L}\right)^2\left(1 + \frac{3}{2}\frac{R}{L}\right)\right\} + O\left(\left(\frac{R}{L}\right)^4\right), \quad (10)$$

with $C_1 \approx 0.125$, $C_2 \approx -0.516$, $C_3 \approx -0.034$. In the same regime, the drag correction in the direction perpendicular to the wall was found to be

$$I_{Dz} = \frac{3}{4}\frac{R}{L} + \frac{9}{16}\left(\frac{R}{L}\right)^2 + \frac{27}{64}\left(\frac{R}{L}\right)^3 + O\left(\left(\frac{R}{L}\right)^4\right). \quad (11)$$

The leading-order term on the right-hand side of (10) is the counterpart of the result derived by Cox & Hsu (1977) for a solid sphere under the assumptions $Re_\infty \ll R/L \ll 1$. Note that this term, as well as the leading-order term on the right-hand side of (11), may be obtained through (A 6) and (A 7) by considering the limit $L^* \to 0$. Terms associated with constants C_1, C_2 and C_3 in (10) represent near-wall

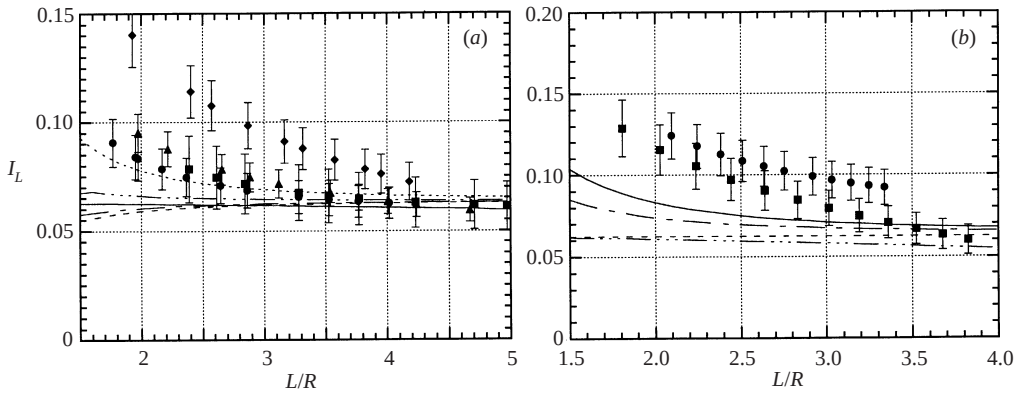

FIGURE 15. (*a*) The wall-induced lift force I_L *vs.* L/R for $Re_\infty = 0.25$ and $L^* < 1$. ■, K10 ($Oh \approx 66$); ●, K20 ($Oh \approx 27$); △, K50 ($Oh \approx 8.7$); ◆, K100 ($Oh \approx 3.4$). Prediction from (10): - - - -, $Re_\infty = 0.25$, $Oh = 6.6$; — - —, $Re_\infty = 0.25$, $Oh = 27$; — · · · —, $Re_\infty = 0.25$, $Oh = 8.7$; · · ·, $Re_\infty = 0.25$, $Oh = 3.4$; ——, prediction from (A 6). (*b*) The wall-induced lift force I_L *vs.* L/R for $L^* < 1$. ●; $Re_\infty = 0.11$ in K100; ■; $Re_\infty = 0.47$ in K100. Prediction from (10): ——, $Re_\infty = 0.11$, $Oh = 2.6$; — - —, $Re_\infty = 0.47$, $Oh = 4.1$. Prediction from (A 6): - - - -, $Re_\infty = 0.11$; — - - - —, $Re_\infty = 0.47$.

corrections of the inertial contribution to the lift force. These corrections arise from higher-order interactions between the flow around the bubble and the wall which become important as the separation L becomes comparable to the radius R. Thus, while (A 6) suggests that the lift force tends to a constant value in the limit of small separations, (10) shows that there is a slight increase of I_L followed by a significant drop as the wall is approached. The last group of terms on the right-hand side of (10) represents the contribution of the deformation to the lift force. Note that this contribution is proportional to $(R/L)^2$, so that it becomes negligible for dimensionless separations of several units.

Here the possible influence of the outer wall of the device may be estimated by comparing (10) with the prediction of Vasseur & Cox (1976) concerning the inertial migration of a solid sphere moving in a quiescent fluid bounded by two parallel walls separated by a gap H. Their result indicates that the most distant wall reduces the transverse force by about 2% for $L/H = 0.12$. Hence we conclude that in the range of L/R of interest here, the influence of the second wall is again very weak, being smaller than the first three terms on the right-hand side of (10).

The experimental determination of I_L in the low-L^* regime is achieved by substituting the measured value of the transverse velocity W and the drag correction (11) corresponding to the local value of L in (3*b*). Figure 15(*a*) shows how the four series of data corresponding to $Re_\infty = 0.25$ in figure 12 ($L^* < 1$) compare with (10). Overall, the data and the theoretical prediction follow the same evolution, but the theory underpredicts systematically the lift force as L/R decreases, the underprediction reaching 30% to 40% for $L/R = 2$. Figure 15(*b*) shows two other typical series of data obtained in the situation $L^* < 1$ which display the same behaviour. The origin of the discrepancy is unclear: the contribution due to deformation in (10) has been derived independently by two different techniques and we checked that if the viscosity of the fluid filling the bubble is made very large, the higher-order corrections to the inertial contribution agree with known results for a rigid sphere (Cherukat & McLaughlin 1994). We are currently investigating this disagreement.

An interesting indication in figures 15(*a*) and 15(*b*) concerns the lowest L^* for which

the description provided by (A 6) applies. Obviously this limit generally depends on the Ohnesorge number. For instance, data corresponding to oils K10, K20 and K50 in figure 15(a) agree with (A 6) for $L^* > 0.4$ whereas the data set $Re_\infty = 0.47$, $Oh = 4.55$ in figure 15(b) shows such an agreement only for $L^* > 0.9$. Consequently, we can conclude that the lowest limit of validity of (A 6) in cases where deformation plays a negligible role in the generation of the lateral force is about $L^* = 0.4$.

5. Summary and concluding remarks

We have described new experimental results concerning the influence of a vertical wall on the evolution of a spherical or spheroidal rising bubble. We have been able to obtain accurate determinations of the drag and lift components of the force as well as of the shape of the bubble by using a travelling optical device combining a CCD camera and a microscope. Another important aspect of the present experiments is the nature of the carrying fluid. Using silicone oils has allowed us to ensure that the bubble surface behaves as a mobile interface; varying the viscosity has made it possible to vary the capillary number for a given rise Reynolds number. We have varied the rise Reynolds number Re_∞ between 0.09 and 32, i.e. we have considered situations in which the flow field around the bubble is dominated by viscous effects as well as cases where inertial effects are dominant.

Qualitatively, the influence of the wall does not change with the Reynolds number in the range covered by the present experiments; the wall is always found to reduce the rise velocity and to produce a repulsive lift force resulting in a migration of the bubble away from it. Moreover, all wall effects increase as the separation L decreases. Nevertheless, experimental results show that, given the relative separation L/R, the strength of these effects strongly decreases as the Reynolds number increases, and becomes insignificant when $Re = O(10)$ or more. This tendency may be explained by the following argument (Legendre & Magnaudet 1998). At low Reynolds number, the vorticity produced by the shear-free condition at the surface of the bubble spreads out and interacts strongly with the wall. In contrast, when inertia effects are dominant, the vorticity is essentially confined in the boundary layer and the wake of the bubble. Interactions between the boundary layer of thickness δ_V and the wall are certainly weak when $(L - R)/\delta_V$ is $O(10)$ or more. Similarly, interactions between the near wake and the wall are necessarily weak because the wake is almost parallel to the wall in the situation considered here, so that the no-slip condition applies in a region of the flow where the velocity defect behind the bubble is almost zero. Consequently, we believe that the distribution of the vorticity around the bubble is responsible for the weak interactions observed for Reynolds numbers of $O(10)$. Moreover, it must be kept in mind that for high enough Reynolds numbers the dominant interaction with the wall results in an attractive lift force. This force, which is an added-mass effect (Milne-Thomson 1968, p. 563), is due to the fact that in potential flow the asymmetry in the velocity distribution around the bubble induces a pressure gradient directed away from the wall. This regime has not been considered here.

Given the weakness of the interactions for $Re_\infty > 1$, most of the analysis has focused on the low-Reynolds-number regime. Following the analyses of Vasseur & Cox (1976, 1977), we found convenient to define two different subregimes, according to the value of the dimensionless separation L^*. Situations with L^* larger than unity correspond to the case where the wall lies in the Oseen region of the flow disturbance. For such situations we have adapted the calculation of Vasseur & Cox (1977) to the case of a shear-free interface in order to determine analytically the wall-induced

drag and lift forces on the bubble. Experimental results obtained in this regime have revealed a good agreement with this theory for Reynolds numbers up to unity and values of L^* larger than 0.4.

Situations in which L^* is smaller than unity, i.e. the wall lies in the Stokes region of the flow disturbance, display a more complex behaviour because when the viscosity of the carrying liquid is large enough, the shear resulting from the relative velocity between the bubble and the wall is able to deform the bubble significantly, thus producing an additional contribution to the lift force. Experimental determinations of the deformation and drag force have been found to compare well with the analytical predictions. In contrast, the measured lift force has been found to increase more than predicted by the theory as the wall is approached.

To complete the description provided by the present investigation and to obtain a clearer view of the mechanisms underlying the various transitions observed here, numerical simulations would be worthwhile. They could also be of great help in obtaining practical expressions for the drag and lift forces for Reynolds numbers between 1 and 10, where experiments have shown that analytical predictions derived under the assumption of low Reynolds number severely underpredict wall-induced effects.

Appendix. Extension of Vasseur & Cox's (1977) result to a clean spherical bubble

Using matched asymptotic expansions, Vasseur & Cox (1977) determined wall effects acting on a solid sphere of radius R moving at a distance L from a plane wall with a velocity U parallel to it. Their analysis is valid provided the condition $R/L \ll UR/v \ll 1$ is satisfied. The first inequality is equivalent to $L^* = LU/v \gg 1$ and indicates that the wall lies in the Oseen region of the flow where viscous and advective effects have a comparable magnitude. In this appendix we extend the result of Vasseur & Cox to the case of a clean spherical bubble. For this purpose we start from the system of equations governing the disturbance flow in the Oseen region. At such distances the first-order effect of the bubble on the flow field can be represented by a point force (Saffman 1965). Then, normalizing distances by v/U, velocities and pressures by RU^2/v and $\rho RU^3/v$ respectively, we obtain the governing equations for the velocity disturbance $\boldsymbol{u}$ and the pressure disturbance p in the form

$$\left.\begin{aligned} &\nabla \cdot \boldsymbol{u} = 0, \\ &\nabla^2 \boldsymbol{u} - \nabla p - \frac{\partial \boldsymbol{u}}{\partial x} = -4\pi(\boldsymbol{e}_x + \alpha \boldsymbol{e}_z)\delta(\boldsymbol{r}), \\ &\boldsymbol{u} \to 0 \quad \text{as} \quad \boldsymbol{r} \to \infty, \\ &\boldsymbol{u} = 0 \quad \text{for} \quad z = -L^*, \end{aligned}\right\} \tag{A 1}$$

where $\delta(\boldsymbol{r})$ is the three-dimensional Dirac distribution, and the strength of the Stokeslet has been chosen to agree with the Hadamard–Rybczynski expression for the drag force on a bubble in the creeping flow regime (Clift *et al.* 1978, p. 33). In (A 1) the angle α between the bubble path and the vertical (x) direction (see figure 4) is assumed to be small, so that the inertia term is neglected in the z-direction. This approximation is based on our experimental results where we observed that α was always less than 0.02, corresponding to a maximum transverse Reynolds number of about 0.1.

As usual in this type of problem we define the two-dimensional Fourier transforms

$$\Gamma_{\mathrm{i}}(k_x,k_y,z)=\frac{1}{4\pi^2}\int_{-\infty}^{\infty}\int_{-\infty}^{\infty}\mathrm{u_i}(\boldsymbol{r})\exp[-\mathrm{i}(k_x x+k_y y)]\,\mathrm{d}x\,\mathrm{d}y,$$

$$\Pi(k_x,k_y,z)=\frac{1}{4\pi^2}\int_{-\infty}^{\infty}\int_{-\infty}^{\infty}p(\boldsymbol{r})\exp[-\mathrm{i}(k_x x+k_y y)]\,\mathrm{d}x\,\mathrm{d}y.$$

Fourier-transforming (A 1) then yields

$$\left.\begin{aligned}&\left\{-k_x^2-k_y^2-\mathrm{i}k_x+\frac{\partial^2}{\partial z^2}\right\}\begin{pmatrix}\Gamma_x\\ \Gamma_y\\ \Gamma_z\end{pmatrix}-\begin{pmatrix}\mathrm{i}k_x\\ \mathrm{i}k_y\\ \partial/\partial z\end{pmatrix}\Pi=-\frac{\delta(z)}{\pi}\begin{pmatrix}1\\0\\ \alpha\end{pmatrix},\\ &\mathrm{i}(k_x\Gamma_x+k_y\Gamma_y)+\partial\Gamma_z/\partial z=0.\end{aligned}\right\}\tag{A 2}$$

Solving (A 2) in the same way as Vasseur & Cox (1977) and taking into account the no-slip condition on the wall, we obtain the Fourier transform of the longitudinal and transverse velocity components at $\boldsymbol{r}=0$ in the form

$$\Gamma_x(0)=\Gamma_x^{\infty}(0)-\frac{1}{2\pi}\left[\frac{\mathrm{i}k_x(t+q)}{q(t-q)}\mathrm{e}^{-2qL^*}+\left\{\frac{2\mathrm{i}k_x t}{(t-q)q}+\frac{\mathrm{i}k_x-1}{t}\right\}\mathrm{e}^{-2tL^*}\right.$$
$$\left.-\frac{4\mathrm{i}k_x t}{(t-q)q}\mathrm{e}^{-(t+q)L^*}\right]-\frac{\alpha}{2\pi}\frac{(t+q)}{(t-q)}(\mathrm{e}^{-qL^*}-\mathrm{e}^{-tL^*})^2,\tag{A 3a}$$

$$\Gamma_z(0)=\Gamma_z^{\infty}(0)+\frac{(t+q)}{2\pi(t-q)}(\mathrm{e}^{-qL^*}-\mathrm{e}^{-tL^*})^2,$$
$$-\frac{\alpha q^2}{2\pi\mathrm{i}k_x(t-q)}\left\{\frac{t+q}{q}\mathrm{e}^{-2qL^*}-4\mathrm{e}^{-(q+t)L^*}+\frac{t+q}{t}\mathrm{e}^{-2tL^*}\right\},\tag{A 3b}$$

where $q^2=k_x^2+k_y^2$, $t^2=q^2+\mathrm{i}k_x$, and $\Gamma_x^{\infty}(0)$ and $\Gamma_z^{\infty}(0)$ denoting the corresponding Oseen solution in unbounded flow. The second term in the right-hand side of (A 3*a*) (resp. (A 3*b*)) is the drag (resp. lift) component of the wall-induced correction due to the wall-parallel velocity U. Similarly the third term in the right-hand sides of (A 3*a*, *b*) is due to the wall-normal velocity W. Consequently this term can be interpreted as a lift (resp. drag) correction in (A 3*a*) (resp. (A 3*b*)). In (A 3*a*) this term is clearly negligible compared to the second one whereas both contributions may have a similar magnitude in (A 3*b*). We now define

$$k_x=\frac{\lambda\cos\phi}{L^*},\quad k_y=\frac{\lambda\sin\phi}{L^*},\quad \lambda=L^*q,\quad \chi(\lambda,\phi)=L^*t.\tag{A 4}$$

Taking the inverse Fourier transform of the second term in the right-hand side of (A 3*a*) and using the above definitions, we obtain the wall-induced velocity correction in the x-direction as

$$I_{Dx}=-\frac{1}{2\pi L^{*2}}\int_0^{\infty}\int_0^{2\pi}\{(\chi+\lambda)\mathrm{e}^{-2\lambda}+2\chi\mathrm{e}^{-2\chi}-4\chi\mathrm{e}^{-(\chi+\lambda)}\}\frac{\mathrm{i}\lambda\cos\phi}{\chi-\lambda}\,\mathrm{d}\lambda\,\mathrm{d}\phi$$
$$-\frac{1}{2\pi L^{*2}}\int_0^{\infty}\int_0^{2\pi}\frac{\mathrm{i}\lambda\cos\phi-L^*}{\chi}\lambda\mathrm{e}^{-2\chi}\,\mathrm{d}\lambda\,\mathrm{d}\phi.\tag{A 5}$$

Similarly, evaluating the inverse Fourier transform of the right-hand side of (A 3*b*)

yields the transverse velocities induced by U and W respectively as

$$I_L = \frac{1}{2\pi L^{*2}} \int_0^{\infty} \int_0^{2\pi} \frac{\chi + \lambda}{\chi - \lambda} (\mathrm{e}^{-\lambda} - \mathrm{e}^{-\chi})^2 \lambda \, \mathrm{d}\lambda \, \mathrm{d}\phi, \tag{A 6}$$

$$\alpha I_{Dz} = -\frac{\alpha}{2\pi L^{*2}} \int_0^{\infty} \int_0^{2\pi} \frac{\lambda^2}{\mathrm{i} \cos\phi} \left\{ \left(\frac{\mathrm{e}^{-2\lambda}}{\lambda} - \frac{\mathrm{e}^{-2\chi}}{\chi} \right) + \frac{2(\mathrm{e}^{-\lambda} - \mathrm{e}^{-\chi})^2}{(\chi - \lambda)} \right\} \mathrm{d}\lambda \, \mathrm{d}\phi. \tag{A 7}$$

In the limit $Re \to 0$ and $L^* \to 0$, (A 5), (A 6) and (A 7) become

$$I_{Dx} = -\frac{3}{8L^*}, \quad I_{Dz} = -\frac{3}{4L^*}, \quad I_L = -\frac{1}{16}. \tag{A 8}$$

These results combined with the Oseen-like expression for the drag force acting on a bubble in an unbounded fluid (Taylor & Acrivos 1964) can be put in dimensional form to obtain the components of the hydrodynamic force in the x- and z-directions as

$$\left.\begin{aligned} F_x &= -4\pi\mu RU \left[1 + \frac{Re}{2} \left(\frac{1}{4} - I_{Dx} \right) \right] = -4\pi\mu RU \left(1 + \frac{Re}{8} + \frac{3}{8} \frac{R}{L} \right), \\ F_x &= -4\pi\mu RU \left[\alpha - \frac{Re}{2} (\alpha I_{Dz} + I_L) \right] = 4\pi\mu R \left[\frac{Re}{32} U - W \left(1 + \frac{3}{4} \frac{R}{L} \right) \right]. \end{aligned} \right\} \tag{A 9}$$

It is worth noting that (A 8) and (A 9) can be recovered directly from the results of Vasseur & Cox (1977) by using the general argument developed by Legendre & Magnaudet (1998). According to this argument, the leading-order correction to the force produced by the wall is $(2/3)^{N+1}$ times that experienced by a solid sphere, N being the number of times the Stokeslet associated with the bubble is involved in the process generating the force. In the present case $N = 1$ because the interaction force results directly from the far-field flow produced by the bubble. In the limit $Re \to 0$ and $L^* \to 0$, Vasseur & Cox (who assumed that the undisturbed motion was parallel to the wall, so that W was zero in their work) found (in our notation) that the correction to F_x was $(27/8)\pi\mu R^2 U/L$ whereas that the lift force was $F_z = (9/32)\pi\mu ReRU$. Multiplying these results by $(2/3)^2$ yields immediately the wall-induced terms of F_x and F_z in (A 9).

REFERENCES

Ambari, A., Gauthier-Manuel, B. & Guyon, E. 1983 Effect of a plane wall on a sphere moving parallel to it. *J. Phys. Lett.* **44**, 143–146.

Batchelor, G. K. 1967 *An Introduction to Fluid Dynamics*. Cambridge University Press.

Benedict, R. P., Abernethy, R. B. & Osolsobe, G. 1985 Measurement uncertainty. *ANSI/ASME Performance Test Code Rep.* 19-1.

Bretherton, F. P. 1962 The motion of rigid particles in a shear flow at low Reynolds number. *J. Fluid Mech.* **14**, 284–304.

Chan, P. C. H. & Leal, L. G. 1979 The motion of a deformable drop in a second-order fluid. *J. Fluid Mech.* **92**, 131–170.

Chan, P. C. H. & Leal, L. G. 1981 An experimental study of drop migration in shear flow between concentric cylinders. *Intl J. Multiphase Flow* **7**, 83–99.

Cherukat, P. & McLaughlin, J. B. 1994 The inertial lift on a rigid sphere in a linear shear flow field near a flat wall. *J. Fluid Mech.* **263**, 1–18.

Clift, R., Grace, J. R. & Weber, M. E. 1978 *Bubbles, Drops and Particles*. Academic.

Cox, R. G. & Hsu, S. K. 1977 The lateral migration of solid particles in a laminar flow near a plate. *Intl J. Multiphase Flow* **3**, 201–222.

Goldman, A. J., Cox, R. G. & Brenner, H. 1967 Slow viscous motion of a sphere parallel to a plane wall. Part I. Motion through a quiescent liquid. *Chem. Engng Sci.* **22**, 637–651.

Happel, J. & Brenner, H. 1973 *Low Reynolds Number Hydrodynamics*. Martinus Nijhoff.

Ho, B. P. & Leal, L. G. 1974 Inertial migration of rigid spheres in two-dimensional unidirectional flows. *J. Fluid Mech.* **65**, 365–400.

Hogg, A. J. 1994 The inertial migration of non-neutrally buoyant spherical particles in two-dimensional shear flows. *J. Fluid Mech.* **272**, 285–318.

Karnis, A. & Mason, S. G. 1967 Particle motion in sheared suspensions. Wall migration of fluid drops. *J. Colloid Sci.* **24**, 164–169.

Leal, L. G. 1980 Particle motions in a viscous fluid. *Annu. Rev. Fluid Mech.* **12**, 435–476.

Leal, L. G. 1992 *Laminar Flow and Convective Transport Processes*. Butterworth-Heinemann.

Legendre, D. & Magnaudet, J. 1997 A note on the lift force on a spherical bubble or drop in a low-Reynolds-number shear flow. *Phys. Fluids* **9**, 3572–3574.

Legendre, D. & Magnaudet, J. 1998 Interaction of two spherical bubbles rising side-by-side. *Proc. 3rd Intl Conf. Multiphase Flow, Lyon, France*.

Magnaudet, J. & Eames, I. 2000 The motion of high-Reynolds-number bubbles in inhomogeneous flows. *Annu. Rev. Fluid Mech.* **32**, 659–708.

Magnaudet, J., Takagi, S. & Legendre, D. 2002 Drag, deformation and lateral migration of a buoyant drop moving near a wall. *J. Fluid Mech.* (submitted).

McLaughlin, J. B. 1991 Inertial migration of a small sphere in linear shear flows. *J. Fluid Mech.* **224**, 261–274.

Mei, R., Klausner, J. F. & Lawrence, C. J. 1994 A note on the history force on a spherical bubble at finite Reynolds number. *Phys. Fluids* **6**, 418–420.

Milne-Thomson, L. M. 1968 *Theoretical Hydrodynamics*. Macmillan.

Moore, D. W. 1963 The boundary layer on a spherical gas bubble. *J. Fluid Mech.* **23**, 749–766.

O'Neill, M. E. & Stewarson, K. 1967 On the slow motion of a sphere parallel to a nearby plane wall. *J. Fluid Mech.* **27**, 706–724.

Saffman, P. G. 1965 The lift force on a small sphere in a slow shear flow. *J. Fluid Mech.* **22**, 385–400.

Shapira, M. & Haber, S. 1988 Low Reynolds number motion of a droplet between two parallel plates. *Intl J. Multiphase Flow* **14**, 483–506.

Shapira, M. & Haber, S. 1990 Low Reynolds number motion of a droplet in shear flow including wall effects. *Intl J. Multiphase Flow* **16**, 305–321.

Smart, J. R. & Leighton, D. T. 1991 Measurement of the drift of a droplet due to the presence of a plane. *Phys. Fluids* A **3**, 21–28.

Stone, H. A. 2000 Philip Saffman and viscous flow theory. *J. Fluid Mech.* **409**, 165–183.

Takemura, F. & Yabe, A. 1998 Gas dissolution process of spherical rising gas bubbles. *Chem. Engng Sci.* **53**, 2691–2699.

Takemura, F. & Yabe, A. 1999 Rising speed and dissolution rate of a carbon dioxyd bubble in slightly contaminated water. *J. Fluid Mech.* **378**, 319–334.

Taylor, G. I. 1934 The formation of emulsions in definable fields on flow. *Proc. R. Soc. Lond.* A **146**, 501–523.

Taylor, T. D. & Acrivos, A. 1964 On the deformation and drag of a falling viscous drop at low Reynolds number. *J. Fluid Mech.* **18**, 466–476.

Uijttewaal, W. S. J. & Nijhof, E. 1995 The motion of a droplet subjected to linear shear flow including the presence of a plane wall. *J. Fluid Mech.* **302**, 45–63.

Uijttewaal, W. S. J., Nijhof, E. & Heethaar, R. M. 1993 Droplet migration, deformation, and orientation in the presence of a plane wall: a numerical study compared with analytical theories. *Phys. Fluids* A **5**, 819–825.

Vasseur, P. & Cox, R. G. 1976 The lateral migration of a spherical particle in two-dimensional shear flows. *J. Fluid Mech.* **78**, 385–413.

Vasseur, P. & Cox, R. G. 1977 The lateral migration of spherical particles sedimenting in a stagnant bounded fluid. *J. Fluid Mech.* **80**, 561–591.